

# Processing and compressive creep of cast replicated IN792 Ni-base superalloy foams

John D. DeFouw\*, David C. Dunand<sup>1</sup>

Department of Materials Science and Engineering, Northwestern University, 2220 N Campus Drive, Evanston, IL 60208, USA

## ARTICLE INFO

### Article history:

Received 18 June 2012

Received in revised form

19 July 2012

Accepted 24 July 2012

Available online 2 August 2012

### Keywords:

Mechanical characterization

Cellular materials

Nickel based superalloys

Casting

## ABSTRACT

Nickel-base superalloy foams were created by a casting replication technique where a lightly sintered preform of SrF<sub>2</sub> was pressure infiltrated with molten IN792; after solidification of the composite, the salt phase was dissolved with HCl to create 65% open porosity. Room temperature yield strength and stiffness of the IN792 foam compared well with existing models. Monolithic and foam samples were tested under creep conditions at 750 and 850 °C at stresses ranging from 5 to 40 MPa for the foams and from 150 to 650 MPa for the monolithic alloy. Both exhibited power-law creep behavior at high stresses and a transition to viscous flow at lower stresses, which was modeled using equations for dislocation and diffusional creep.

© 2012 Elsevier B.V. All rights reserved.

## 1. Introduction

Metallic foams offer several advantages for engineering applications necessitating reduced density and high specific strength and modulus as compared to monolithic materials [1–3]. For high temperature applications requiring corrosion, oxidation and creep resistance together with high ductility and toughness, Ni-base superalloys remain unmatched. Nickel alloy foams have been processed by chemical vapor deposition of Cr and Al onto commercial Ni foam followed by homogenization [4,5], compaction of pre-alloyed powders together with a spaceholder material that is burned off prior to sintering of the powders [6,7], electron beam deposition of the alloy onto an organic template followed by burn off and sintering [8], and casting replication around a dissolvable oxide spaceholder [9,10]. Many of these alloys – Hastelloy X, Hastelloy C, IN625, IN600, J5, Ni–Cr, and Ni–Cr–Al – have good strength, oxidation, and corrosion resistance but lack the combination of these properties with the creep resistance displayed by nickel-base superalloys such as IN792 (Ni–12.6Cr–9.0Co–1.9Mo–4.3W–4.3Ta–3.4Al–4.0Ti–1.0Hf–0.09C–0.02B–0.06Zr, wt% [11]), which are highly alloyed and contain a large volume fraction of  $\gamma'$  (Ni<sub>3</sub>Al-based) precipitates.

Here, we show that the Ni-base superalloy IN792 can be processed into an open-celled metallic foam using the casting replication method with dissolvable SrF<sub>2</sub> spaceholder and we measure and model the foam compressive properties at an ambient and elevated temperature.

## 2. Experimental procedures

### 2.1. Processing

SrF<sub>2</sub> was selected as space-holder because of its very high melting temperature ( $T_m=1473$  °C [12]) in excess of the liquidus temperature (1325–1350 °C [13]) of the commercial superalloy IN792. Powders of SrF<sub>2</sub> were created by grinding photonic-grade crystals of SrF<sub>2</sub> (Alfa Aesar, MA) with mortar and pestle and sieving to 355–700  $\mu\text{m}$  particle size. The monocrystalline powder was poured into an alumina crucible (ID $\sim$ 7 mm) and sintered under an Ar atmosphere at 1400 °C for 10 h. A porous alumina spacer disc was placed onto the pattern with an IN792 cylinder (7 mm in diameter, 40 mm in length, and weighing 12.7 g). The alloy was melted by heating at 7 °C/min to 1450 °C under high vacuum ( $6 \times 10^{-4}$  Pa), held 30 min at that temperature and forced into the preform by application of 1 atm Ar. After solidification and furnace cooling, the IN792/SrF<sub>2</sub> composite was machined to cylindrical samples (6 mm diameter, 12 mm length), and placed in an ultrasonically agitated 5 vol% HCl bath to dissolve the salt phase. The samples were removed periodically to measure their density through helium pycnometry to determine the extent of dissolution (at full dissolution, density of the

\* Corresponding author. Present address: Department of Materials Science and Engineering, The Ohio State University, 105 W Woodruff Avenue, Columbus, OH 43201, USA. Tel.: +1 614 247 6696; fax: +1 614 292 1537.

E-mail addresses: [defouw.2@osu.edu](mailto:defouw.2@osu.edu) (J.D. DeFouw), [dunand@northwestern.edu](mailto:dunand@northwestern.edu) (D.C. Dunand).

<sup>1</sup> Tel.: +1 847 491 5370; fax: +1 847 467 6573.

open cell foam reaches to that of the monolithic alloy). Monolithic samples (4 mm diameter, 8 mm length) were machined from a cast ingot. Porous and monolithic samples were heat-treated according to Ref. [13] by first solutionizing at 1120 °C for 4 h followed by water quenching. Precipitation of the  $\gamma'$  phase was achieved by a double aging procedure: 1080 °C/4 h, water quenching and 845 °C/24 h water quenching.

## 2.2. Characterization

The as-processed foam was imaged using scanning electron microscopy (SEM) to observe the macroscopic structure of pores after removal of SrF<sub>2</sub>. Further samples were mounted in epoxy and polished using standard metallographic procedures down to a 1  $\mu$ m diamond finish. To observe the  $\gamma'$  precipitate structure, a sample was etched with 10 ml hydrofluoric and 100 ml nitric acid solution and imaged using SEM. The cast dendritic structure was imaged by optical microscopy after etching with a dilute HF aqueous solution.

## 2.3. Mechanical testing

A cylindrical foam sample (6 mm in diameter and 12 mm in length) was tested in compression using a MTS 810 system with laser extensometer at ambient temperature. The sample was loaded to a target strain and then unloaded to 10 MPa before loading to a higher strain again. Elastic stiffness was measured on periodic unloading to determine damage accumulation. Unloading was performed at 12 total intervals during the compression test.

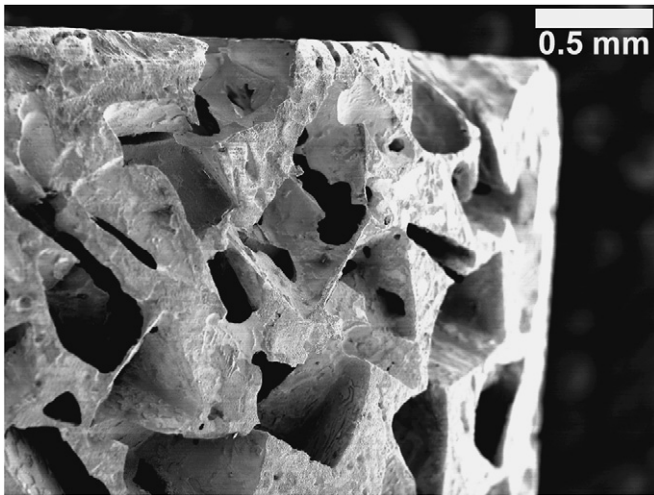


**Fig. 1.** Scanning electron microscopy image of IN792 foam after dissolution of the SrF<sub>2</sub> spaceholder. Pores have the sharp polygonal morphology of the SrF<sub>2</sub> powders.

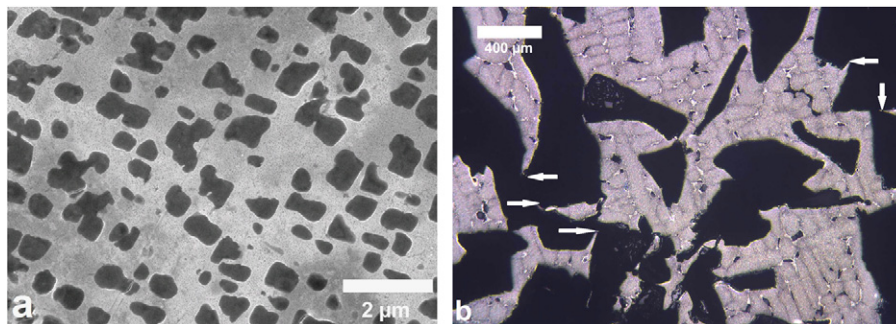


**Fig. 2.** Polished cross-sections showing microstructure of IN792 foam with (a)  $\gamma'$  precipitates (scanning electron micrograph) and (b) uniform dendrite pattern and no grain boundaries with arrows indicating unconnected struts resulting from incomplete infiltration (optical micrograph).

Compressive creep testing was performed on a compressive frame (Applied Test Systems, PA) at constant stress at 750 and 850 °C with linear voltage displacement transducer monitoring the platen displacement. Foam samples were cylindrical with 6 mm diameter and 12 mm length and monolithic samples were cylindrical with 4 mm diameter and 8 mm length. Multiple increasing stress levels were tested on a single sample if a minimum creep rate was met before extensive deformation of the sample.

## 3. Results

### 3.1. Density and microstructure

The IN792 alloy foams had an average density of 2.89 g/cm<sup>3</sup> which was 35% of the monolithic alloy density of 8.25 g/cm<sup>3</sup>. Pores replicated the sharp polygonal shape of the ground SrF<sub>2</sub> powders which created thick nodes and thin struts as shown in Fig. 1. Since negligible dissolution of the alloy takes place during dissolution of the spaceholder, the pore size is assumed to remain in the range 355–700  $\mu$ m. Foams exhibited the creep-resistant  $\gamma'$  precipitates as shown in Fig. 2a, as well as a coarse grain structure, as inferred from Fig. 2b showing uniform dendrite orientation over millimeter-wide areas with no visible grain boundaries after etching.

### 3.2. Ambient temperature compression

Under uniaxial compression at room temperature, the stress–strain curve of the foam (shown in Fig. 3) exhibited a elastic response with a stiffness of 13 GPa and a yield stress of  $\sim$ 70 MPa, followed by a region where the stress increases near uniformly with strain, as often exhibited by salt-replicated metallic foams [14,15], but unlike the plateau stress typical of higher porosity metallic foams [2]. The foam failed mechanically at a strain of  $\sim$ 70%. Through periodic unloading of the sample during the test to measure stiffness vs. strain, damage is seen up to a 10% strain as a 25% reduction in stiffness. Beyond 20% strain, the stiffness increases as the material densifies.

### 3.3. Compressive creep

Monolithic and foam samples exhibited a typical primary creep with decreasing strain rate followed by a long region of secondary creep with a minimum strain rate constant over long time periods. The minimum creep strain rate is plotted against the applied stress in Fig. 4 for both monolithic and foam samples. Most data follow a power-law behavior described by

$$\dot{\epsilon} = A\sigma^n \exp\left(\frac{-Q_p}{RT}\right) \quad (1)$$

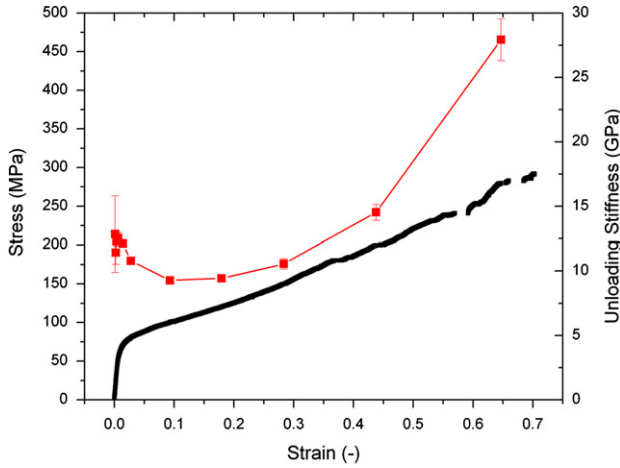


**Fig. 3.** Stress vs. strain curve for 35% dense IN792 foam during compressive deformation and unloading stiffness vs. strain plot. Missing data are due to the laser extensometer losing signal.

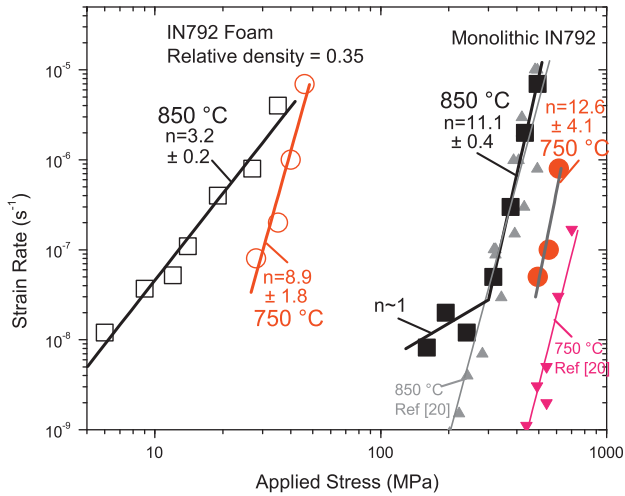


**Fig. 4.** Double logarithmic plot of creep strain rate vs. applied stress for monolithic IN792 alloy (filled symbols) and IN792 alloy foams (open symbols) compressively deformed at 750 and 850 °C. Stress exponents are given next to each data set. Literature data from Ref. [20] for creep of monolithic IN792 are shown for comparison.

where  $\dot{\epsilon}$  is the strain rate,  $A$  is the Dorn constant,  $\sigma$  is the applied stress,  $n$  is the stress exponent,  $Q_p$  is the activation energy,  $R$  the gas constant and  $T$  the temperature. Foam samples of the IN792 alloy had best-fit stress exponents of  $8.9 \pm 1.8$  at 750 °C and  $3.2 \pm 0.2$  at 850 °C. At 750 °C, monolithic samples exhibited a best-fit stress exponent of  $12.6 \pm 4.1$  while samples tested at 850 °C had a stress exponent of  $11.1 \pm 0.4$  at stresses over 300 MPa but a transition to near  $n \sim 1$  for stresses below 300 MPa. The value  $n \sim 1$  is assumed here, but it is in general agreement with the fit to the three data points in this region which gave  $n = 0.9 \pm 2$  (the large error is due to low number of points).

## 4. Discussion

### 4.1. Density and microstructure

The relative density of 0.35 is low considering packing of these types of particles should typically reach only  $\sim 50\%$  [16]. The low relative density could be caused by improved packing due to the sintering of the SrF<sub>2</sub>. This was observed in similar experiments with a Ni-alloy of different chemistry and with smaller size SrF<sub>2</sub> where

the resulting foams had a relative density of 0.40 [17]. The low density here could also be caused by incomplete infiltration which can be visualized by unconnected struts in Fig. 2b. Higher infiltration pressures or larger sized SrF<sub>2</sub> particles (reducing internal capillary forces) could resolve this issue. Despite the presence of the SrF<sub>2</sub> surface as a nucleation source, the material showed no grain boundaries in sections analyzed and appears coarse-grained. The low thermal conductivity of SrF<sub>2</sub> may have prevented excessive heterogeneous nucleation as the metal cooled faster.

### 4.2. Ambient temperature compression

Using existing models for foam compressive behavior [2], both foam elastic stiffness and yield strength can be estimated from monolithic properties. The foam elastic stiffness,  $E_f$ , can be calculated from Eq. (2) where  $C_E$  is a scaling constant between 0.1 and 1,  $E_s$  is the elastic Young's modulus of the monolithic (solid) material and  $\rho^*$  is the relative density:

$$E_f \approx C_E E_s \rho^{*2} \quad (2)$$

Given a monolithic Young's modulus of 200–210 GPa for highly alloyed Ni-base superalloys [18,19], a scaling constant  $C_E \sim 0.5$  fits the value of 13 GPa; the present value of  $C_E$  is in the typical range of 0.1–1 but lower than for another Ni-base alloy with  $C_E \sim 1$  produced by a similar method [9] although near that of Zr-base alloys produced by replication with  $C_E \sim 0.3$  [16]. The difference between these constants is probably due to the geometry of the metal struts, dictated by the dissolvable spaceholder. The IN792 here and Zr-base alloy used sharp polygonal pieces ground from fluoride salts leading to struts that are very thin as compared to the nodes, or in some cases unconnected (Fig. 2b). By contrast, the Ni-base alloy in Ref. [9] used an oxide spaceholder that was sintered from fine particles and then ground producing a more rounded shape, and more uniform strut cross-sections.

The yield strength,  $\sigma_{yf}$ , can be estimated from Eq. (3) where  $C_\sigma$  is a scaling constant around 0.3,  $\sigma_{ys}$  is the yield strength of the monolithic material and  $\rho^*$  is again the relative density:

$$\sigma_{yf} \approx C_\sigma \sigma_{ys} \rho^{*3/2} \quad (3)$$

The yield strength predicted by Eq. (3) with  $C_\sigma = 0.3$  and monolithic yield strength of 1060 MPa [18] is 66 MPa, close to the measured value of 70 MPa.

The damage evolution observed through reductions in stiffness (Fig. 3) is similar to that reported in a 14% relative density aluminum foam [15] also produced through a salt replication casting method. Although strength and modulus differ greatly, minimum stiffness occurred at 10% strain followed by increase in stiffness during densification of the foam. The present superalloy foam lost  $\sim 25\%$  of its modulus compared to about 50% for the aluminum foam, suggesting that less damage was accumulated in the superalloy foam possibly because its relative density is much higher than that for the pure aluminum foam (35% vs. 14%).

### 4.3. Compressive creep

As shown in Fig. 4, the present monolithic IN792 creep data agree well with the data presented for cast IN792 in Ref. [20], except for the transition to a low stress exponent  $n \sim 1$  below an applied stress of 300 MPa at 850 °C which is expected to be associated with diffusional creep and is thus dependent on grain size. The strain rate  $\dot{\epsilon}$  in this regime is given in Ref. [21] as follows:

$$\dot{\epsilon} = \frac{14.3 \Omega \sigma D_{eff}}{\kappa T d^2} \quad (4)$$

where  $\Omega$  is the atomic volume,  $d$  is the grain size,  $\kappa$  is the Boltzman constant,  $T$  the temperature, and the effective diffusion coefficient

$D_{eff}$  is represented by

$$D_{eff} = D_v \left( 1 + \left( \frac{\pi}{d} \right) \left( \frac{D_{gb}}{D_v} \right) \right) \quad (5)$$

where  $D_v$  is the volume diffusion and  $D_{gb}$  the grain boundary diffusion. As both mechanisms are independent, the total creep rate of the material is given by adding the power-law contribution (Eq. (1)) and the diffusional contribution (Eq. (4)):

$$\dot{\epsilon} = A\sigma^n \exp\left(\frac{-Q_p}{RT}\right) + \frac{14.3\Omega\sigma D_{eff}}{\kappa T d^2} \quad (6)$$

Grain size was not measured, so Eq. (6) was fit to the creep data, using materials parameters from Ref. [21] for Mar-M-200 (an alloy similar to IN792) and  $d$  as an adjustable parameter; the transition between the two regimes occurs at stresses near 300 MPa, with a reasonable grain size of 150–200  $\mu\text{m}$ . With this range of grain size and a small range in stress exponent (11.1–11.2 at 850 °C and 12.6–12.7 at 750 °C), the experimental creep data is enveloped by Eq. (6), as illustrated in Fig. 5.

The foam creep strain rate  $\dot{\epsilon}_f$  can be described similarly by adding equations for foam diffusional and power law creep from Ref. [2]

$$\dot{\epsilon}_f = A \frac{0.6}{(n+2)} \left( \frac{1.7(2n+1)}{n} \right)^n \sigma_f^n \rho^{*-(3n+1)/2} \exp\left(\frac{-Q_p}{RT}\right) + \frac{14.3\Omega\sigma_f \rho^{*-2} D_{eff}}{\kappa T d^2} \quad (7)$$

This model assumes deformation by strut bending which is credible given the large node and thin strut morphology seen in Figs. 1 and 2. According to Eq. (7), a foam has the same stress exponent as the monolithic material. At first sight, Fig. 4 shows significant differences in the creep exponents between dense and porous materials:  $n=12.6 \pm 4.1$  and  $n=8.9 \pm 1.8$  respectively at 750 °C and  $n=11.1 \pm 0.4$  and  $n=3.2 \pm 0.2$  at 850 °C. However, as shown in Fig. 6, it is possible to use Eq. (7) to envelop the foam experimental data at 750 °C using the same range of grain size of 150–200  $\mu\text{m}$  as for the monolithic. The large discrepancy in the stress exponent at 850 °C disappears if the grain size is allowed to span a slightly wider range of 50–200  $\mu\text{m}$ , as shown in Fig. 6. The low stress exponent  $n=3.2 \pm 0.2$  in the foam is then interpreted as resulting from a sample with a wider range of stable grain

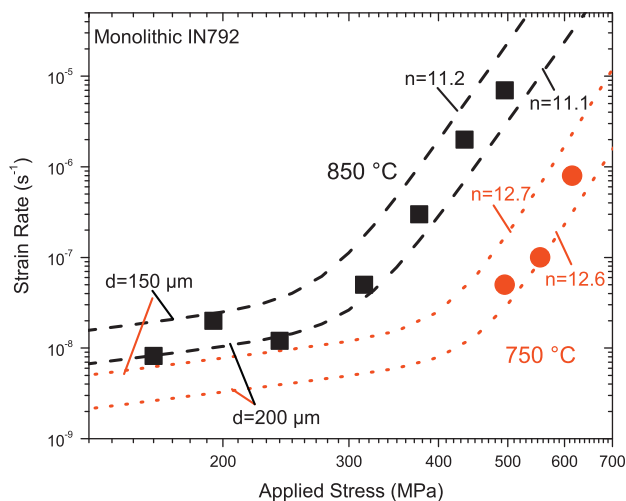


**Fig. 5.** Double logarithmic plot of compressive creep strain rate vs. stress for IN792 monolithic samples, with dashed lines from Eq. (6) showing encapsulation of data at 850 °C with stress exponent  $n=11.1$ –11.2 (monolithic value  $n=11.1$ ) and grain size  $d=150$ –200  $\mu\text{m}$ . Data from creep at 750 °C are similarly encapsulated with  $n=12.6$ –12.7 and  $d=150$ –200  $\mu\text{m}$ .

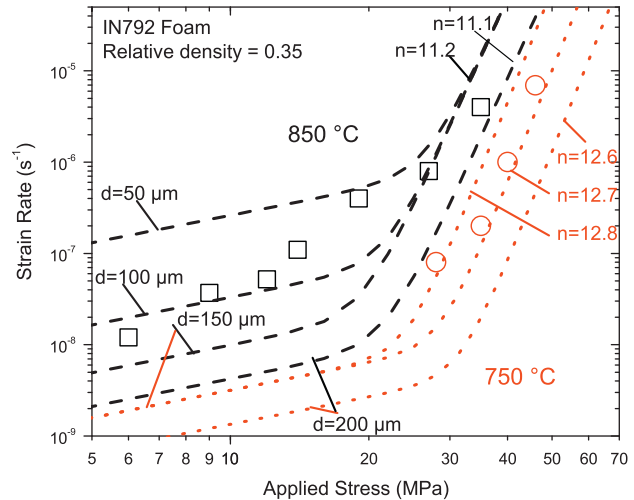


**Fig. 6.** Double logarithmic plots of compressive creep strain rate vs. stress for IN792 foams at 750 °C and 850 °C, with dashed lines from Eq. (7). Although best-fit foam stress exponents shown in Fig. 5 were different from monolithic value, due to the transition from diffusional creep to dislocation creep, monolithic stress exponents ( $n=11.1$ –11.2 at 850 °C and  $n=12.6$ –12.8 at 750 °C) and grain sizes ( $d=50$ –200  $\mu\text{m}$  at 850 °C and  $d=150$ –200  $\mu\text{m}$  at 750 °C) can also be used to describe the foam behavior.

sizes. Assuming that grains are pinned by the pores as bamboo grains, such a broader range is credible in the foam showing coarse nodes and fine struts with coarse grains and fine grains, respectively. Also, the range of stresses locally in the foam is much higher than in the bulk, due to stress concentrations, again providing a qualitative justification for the broad range of stresses where the transition between the two types of mechanism appears to occur for the foam. Diffusional creep may further be affected by the flow of vacancies to and from pore surfaces; this mechanism, which is not expected to affect the stress exponent of unity may impact the activation energy of viscous flow, is not considered further here. Although grain boundaries were not visible by metallography, it would be expected for the foam to have a smaller grain size than monolithic if the spaceholder particles act as nucleation sites. A similar situation was observed in Ni–Cr foams [4], where the foam had a lower stress exponent ( $n=3.3$ –3.7) than the monolithic material ( $n=4.6$ ) and was also likely tested in the stress range where a broad transition from power-law to diffusional creep occurred.

Many of the studies of Ni-alloy foams have focused on processing (as reviewed in Section 1), with only a few performing creep experiments. In these studies [4,5,10], the foams were made from Ni–Cr, Ni–Cr–Al, and J5 alloys, which are not designed to be as creep resistant as the highly alloyed IN792 used here, and show lower power-law stress exponents at lower temperatures (680–850 °C). In the case of J5 [9], a Ni–22.5Mo–12.5Cr–1Ti–0.5Mn–0.1Al–0.1Y alloy designed for solid oxide fuel cells, the foam relative density was 0.46 and exhibited a minimum creep rate at 850 °C similar to that of the IN792 foam studied here, which has a significantly lower relative density of 0.35 and much better oxidation resistance. This illustrates the benefit in using a highly alloyed, precipitation-strengthened Ni-base superalloy for creep resistant foams.

## 5. Conclusions

A Ni-base superalloy alloy IN792 foam was created by a cast replication technique, where the liquid alloy was pressure infiltrated into a bed of  $\text{SrF}_2$  powders, which were removed after alloy solidification using a 5% HCl solution. The foam, with an open

porosity of 65%, exhibited a stiffness of 13 GPa and yield strength of 70 MPa at room temperature, in agreement with existing models for foams deforming by strut bending. Both monolithic and foam samples were tested under creep conditions at 750 and 850 °C. Monolithic alloy exhibited power-law behavior at high stress, with stress exponents of 11.1 and 12.6 at 850 and 750 °C respectively. At stresses below ~300 MPa, diffusional creep was observed with stress exponent near unity. Both regimes can be modeled using existing equations for power-law and diffusional creep. The foam exhibited power-law behavior with stress exponents of 3.2 and 8.9 at 850 and 750 °C respectively, different from monolithic values. However, their creep behavior can be described with existing foam creep models using data from monolithic testing, assuming that the lower stress exponents reflects a diffuse transition from diffusional to dislocation creep, reflecting a range of grain size.

### Acknowledgments

The authors thank Mr. Nirand Pisutha-arnond (Northwestern University, supported in part by an undergraduate research grant from the Ford Motor Company) for assistance with pressure infiltration experiments and microscopy. Part of this research was funded by NASA through a subcontract from GE (award NNC06CB31C) and supervised by Dr. R. Bhat (GE Global Research Center).

### References

- [1] M.F. Ashby, T. Evans, N.A. Fleck, L.J. Gibson, J.W. Hutchinson, H.N.G. Wadley, *Metal Foams: A Design Guide*, Butterworth-Heinemann, Boston, 2000.
- [2] L.J. Gibson, M.F. Ashby, *Cellular Solids: Structure and Properties*, Cambridge University Press, 1997.
- [3] L.P. Lefebvre, J. Banhart, D.C. Dunand, *Adv. Eng. Mater.* 10 (2008) 775–787.
- [4] H. Choe, D.C. Dunand, *Mater. Sci. Eng. A* 384 (2004) 184–193.
- [5] H. Choe, D.C. Dunand, *Acta Mater.* 52 (2004) 1283–1295.
- [6] M. Bram, C. Stiller, H.P. Buchkremer, D. Stover, H. Baur, *Adv. Eng. Mater.* 2 (2000) 196–199.
- [7] P. Quadbeck, J. Kaschta, R.F. Singer, *Adv. Eng. Mater.* 6 (2004) 635–639.
- [8] T.D. Queheillalt, D.D. Hass, D.J. Sypeck, H.N.G. Wadley, *J. Mater. Res.* 16 (2001) 1028–1036.
- [9] Y. Boonyongmaneerat, D.C. Dunand, *Adv. Eng. Mater.* 10 (2008) 379–383.
- [10] Y. Boonyongmaneerat, D.C. Dunand, *Acta Mater.* 57 (2009) 1373–1384.
- [11] T.M. Pollock, S. Tin, *J. Propul. Power.* 22 (2006) 361–374.
- [12] Chemical Rubber Company, *CRC Handbook of Chemistry and Physics*, CRC Press, Cleveland, 1977.
- [13] J.K. Tien, T. Caulfield, *Superalloys, Supercomposites and Superceramics*, Academic Press, Boston, 1989.
- [14] C. San Marchi, A. Mortensen, *Acta Mater.* 49 (2001) 3959–3969.
- [15] J. Despois, R. Mueller, A. Mortensen, *Acta Mater.* 54 (2006) 4129–4142.
- [16] A.H. Brothers, D.C. Dunand, *Adv. Mater.* 17 (2005) 484–486.
- [17] M.L. Young, J.D. DeFouw, J. Frenzel, D.C. Dunand, *Metall. Mater. Trans. A* 43 (2012) 2939–2944.
- [18] ASM Handbook Committee on Properties and Selection: Stainless Steels, Tool Materials and Special-Purpose Metals, 9th ed., *Metals Handbook*, vol. 3, ASM, Metals Park, 1980.
- [19] M.J. Donachie, S.J. Donachie, *Superalloys: A Technical Guide*, 2nd edition, ASM, Metals Park, 2002.
- [20] P. Almroth, M. Hasselqvist, K. Simonsson, S. Sjöström, *Comp. Mater. Sci.* 29 (2004) 437–445.
- [21] H.J. Frost, M.F. Ashby, *Deformation-Mechanism Maps: The Plasticity and Creep of Metals and Ceramics*, Pergamon Press, New York, NY, 1982.